

## Article

# The Study on the Active Site Regulated $\text{RuO}_x/\text{Sn}_{0.2}\text{Ti}_{0.8}\text{O}_2$ Catalysts with Different Ru Precursors for the Catalytic Oxidation of Dichloromethane

Yang Yang <sup>1,\*</sup>, Zhong Zheng <sup>1</sup>, Mengyue Kong <sup>2</sup>, Zhesheng Hua <sup>1</sup>, Zhengda Yang <sup>3</sup>, Ye Jiang <sup>3</sup>, Shaojun Liu <sup>1</sup> , Xinhuan Yan <sup>2,\*</sup> and Xiang Gao <sup>1</sup>

<sup>1</sup> Institute for Thermal Power Engineering, Zhejiang University, Hangzhou 310027, China; 21927034@zju.edu.cn (Z.Z.); 21927085@zju.edu.cn (Z.H.); phoenix205@zju.edu.cn (S.L.); xgao1@zju.edu.cn (X.G.)

<sup>2</sup> College of Chemical Engineering, Zhejiang University of Technology, Hangzhou 310014, China; mykong2015@126.com

<sup>3</sup> College of New Energy, China University of Petroleum (East China), Qingdao 266580, China; yzd019@upc.edu.cn (Z.Y.); jiangye@upc.edu.cn (Y.J.)

\* Correspondence: 11527077@zju.edu.cn (Y.Y.); xhyan@zjut.edu.cn (X.Y.)



**Citation:** Yang, Y.; Zheng, Z.; Kong, M.; Hua, Z.; Yang, Z.; Jiang, Y.; Liu, S.; Yan, X.; Gao, X. The Study on the Active Site Regulated  $\text{RuO}_x/\text{Sn}_{0.2}\text{Ti}_{0.8}\text{O}_2$  Catalysts with Different Ru Precursors for the Catalytic Oxidation of Dichloromethane. *Catalysts* **2021**, *11*, 1306. <https://doi.org/10.3390/catal11111306>

Academic Editors: Zhenghua Tang, Marc Cretin and Sophie Tingry

Received: 27 September 2021

Accepted: 25 October 2021

Published: 28 October 2021

**Publisher's Note:** MDPI stays neutral with regard to jurisdictional claims in published maps and institutional affiliations.



**Copyright:** © 2021 by the authors. Licensee MDPI, Basel, Switzerland. This article is an open access article distributed under the terms and conditions of the Creative Commons Attribution (CC BY) license (<https://creativecommons.org/licenses/by/4.0/>).

**Abstract:** Chlorine-containing volatile organic compounds (CVOCs) present in industrial exhaust gas can cause great harm to the human body and the environment. In order to further study the catalytic oxidation of CVOCs, an active site regulated  $\text{RuO}_x/\text{Sn}_{0.2}\text{Ti}_{0.8}\text{O}_2$  catalyst with different Ru precursors was developed. With Dichloromethane as the model molecule, the activity test results showed that the optimization of Ru precursor using Ru colloid significantly increased the activity of the catalyst ( $T_{90}$  was reduced by about 90 °C when the Ru loading was 1 wt%). The analysis of characterization results showed that the improvement of the catalytic performance was mainly due to the improvement of the active species dispersion (the size of Ru cluster was reduced from 3–4 nm to about 1.3 nm) and the enhancement of the interaction between the active species and the support. The utilization efficiency of the active components was improved by nearly doubling TOF value, and the overall oxidation performance of the catalyst was also enhanced. The relationship between the Ru loading and the catalytic activity of the catalyst was also studied to better determine the optimal Ru loading. It could be found that with the increase in Ru loading, the dispersibility of  $\text{RuO}_x$  species on the catalyst surface gradually decreased, despite the increase in their total amount. The combined influence of these two effects led to little change in the catalytic activity of the catalyst at first, and then a significant increase. Therefore, this research is meaningful for the efficient treatment of CVOCs and further reducing the content of active components in the catalysts.

**Keywords:** air pollution; dichloromethane; catalytic oxidation; Ru; colloid

## 1. Introduction

Chlorine-containing volatile organic compounds (CVOCs) are widely present in waste gas emitted by industries such as dry cleaning, medicine, organic synthesis, and metal processing [1–4]. CVOCs is listed as one of the culprits of the atmospheric ozone hole and promotes the generation of haze and photochemical smog. Due to its strong toxicity and bioaccumulation, CVOCs will cause great harm to the human body as well. Therefore, many CVOCs have been listed as priority pollutants by the United States, China and many other countries [5–8]. The catalytic combustion method is considered to be an advanced technology that can effectively eliminate CVOCs due to its advantages of low ignition temperature, low energy consumption, high removal efficiency, and small secondary pollution [9,10]. Because the existing catalysts generally face problems such as low catalytic activity and poor chlorine poisoning resistance, the development of efficient and stable catalysts is at the core of catalytic combustion process research [11].

The important reason of chlorine poisoning deactivation of the catalyst is that the Cl species adsorbed on the surface of the catalyst is difficult to remove in a sufficient time-frame, thus blocking the active sites of the catalyst [9,12]. Ru-based catalysts are widely used in heterogeneous catalysis, including the decomposition of various organic compounds [13,14] and the oxidation of carbon monoxide [15,16], due to their excellent redox performance. At the same time, because of the unique promotion of Ru species to Deacon reaction ( $4\text{HCl} + \text{O}_2 = 2\text{Cl}_2 + 2\text{H}_2\text{O}$ ) [17], Ru-based catalyst possess great stability under HCl/Cl<sub>2</sub> conditions. Therefore, the introduction of Ru species is expected to significantly improve the chlorine poisoning resistance and oxidation performance of the catalyst. In addition, the acidic sites on the surface of the catalyst can effectively adsorb and activate the C-Cl bonds of the CVOC molecules, thereby improving the low-temperature catalytic activity of the catalyst [10,18,19]. Our previous study found that Sn<sub>0.2</sub>Ti<sub>0.8</sub>O<sub>2</sub> support could not only provide sufficient Lewis acid sites, but also effectively solve the problem of Ru species aggregation by contributing to the epitaxy growth of Ru species on its surface due to its rutile crystal form [20]. With further in-depth research, how to further improve the catalytic activity of the catalyst, reduce the active component Ru loading, and reduce the cost of catalyst preparation has become a major problem that needs to be overcome.

Many methods aimed at increasing the catalytic activity of catalysts essentially increase the total number of active sites on the catalyst surface. The total number of active sites on the catalyst surface is related to many factors. First, increasing the content of active components on the catalyst can increase the total number of active sites to a certain extent [21]. However, not all the loaded active components are highly active, if the active components are aggregated on the catalyst surface, the total number of active sites may be far less than the active component loading [22], so the dispersibility of the active components should also be considered. The optimization of the catalyst preparation method can significantly improve the physical and chemical properties of the catalyst [23]. Studies have shown that pre-preparing precious metals such as Ag, Au, Pt and Pd into nanoparticles before loading them can significantly improve the dispersion of active components and improve the utilization efficiency of active components [21,24–28]. In addition, the improvement of support crystal types [20] and the addition of specific anchor sites [29,30] can effectively promote the dispersion of active components and prevent their agglomeration.

In this paper, we optimized the Ru precursor and used Sn<sub>0.2</sub>Ti<sub>0.8</sub>O<sub>2</sub> as support to prepare efficient and stable CVOCs catalysts. Using DCM (dichloromethane) as the model molecule, differences in catalytic activity between the catalysts using different Ru precursors under the same RuO<sub>x</sub> loading condition was compared, and the physical and chemical properties of the catalyst were analysed by a variety of characterization analysis methods. In addition, in order to select the optimal RuO<sub>x</sub> loading more scientifically and efficiently, we adjusted the RuO<sub>x</sub> loading to study the specific relationship between the catalytic performance of the catalyst and the RuO<sub>x</sub> content.

## 2. Experimental Section

### 2.1. Catalyst Preparation

Sn<sub>0.2</sub>Ti<sub>0.8</sub>O<sub>2</sub> support was prepared by using the co-precipitation method. A certain amount of SnCl<sub>4</sub> and tetrabutyl titanate (TBT) was added into deionized water. After full stirring, 25% ammonia solution was added to adjust the pH to 10. After 12 h of aging, the precipitate was dried, ground, and calcined at 500 °C for 5 h to obtain the final support (which was named as ST).

The o-1-RuST sample was obtained by loading Ru through the traditional impregnation method. The support powder was added after mixing an appropriate amount of RuCl<sub>3</sub> precursor solution and quantificational 15% hydrogen peroxide solution under the condition of 95 °C water bath. The catalyst with 1 wt% Ru loading was evaporated, dried, ground, and calcined at 500 °C for 5 h. In order to further confirm the significant

improvement in the catalytic performance by the optimization of Ru precursor, we also prepared the o-5-RuST sample with a Ru loading of 5 wt% for catalytic activity comparison.

Three samples with Ru mass fractions of 0.1 wt%, 0.5 wt% and 1 wt% were obtained by loading Ru through Ru colloid solution, which was named c-0.1-RuST, c-0.5-RuST and c-1-RuST, respectively. The preparation method of Ru colloidal solution is as follows: The precursor  $\text{RuCl}_3$  was dissolved in propylene carbonate solution at a concentration of 0.3 mg/mL. Then, PVP (Polyvinylpyrrolidone) with a molar ratio of 20:1 to  $\text{RuCl}_3$  and Triethylamine with a molar ratio of 10:1 to  $\text{RuCl}_3$  were added. After fully stirring, transferred the solution to the autoclave, passed hydrogen to 8 MPa, heated to 30 °C and reacted for 2 h to obtain the desired colloid solution. The Ru colloid solution was then taken with different content and fully mixed with the support powder, evaporated, dried, ground, and calcined at 500 °C for 5 h to obtain the three samples with different Ru contents.

The chemical reagents used in the preparation of the catalyst are shown in Table S1.

## 2.2. Catalyst Characterization

XRF characterization using Bruker D8 Advance (Bruker, Berlin, Germany) was performed to measure the actual content of Ti and Ru in the catalyst. The D2 PHASER (Bruker, Berlin, Germany) crystal diffractometer was used for XRD characterization to quantitatively and qualitatively analyse the phase parameters of the catalyst. XPS technique with the equipment of Thermo ESCALAB 250XI (Waltham, MA, America) was used to determine the valence distribution of Ru and O elements on the surface of the catalyst, and the binding energy of all elements was calibrated with C 1 s at 284.8 eV as the standard. TEM-mapping was used to characterize and observe the catalyst particle size and surface element dispersion, and the instrument model was JEOL 2100F TEM/STEM (Tokyo, Japan). The size of Ru clusters in each sample was further observed using a spherical aberration-corrected transmission electron microscope, the model of which was Titan ChemiSTEM (Thermo fisher, Waltham, MA, America). An AutoChem II 2920 (Micromeritics, GA, America) model of automatic temperature programmed chemical adsorption instrument was used performed  $\text{H}_2$ -TPR characterization to determine the oxidation-reduction performance and the metal dispersion of the catalysts. After pre-treatment and purging,  $\text{H}_2$ -TPR was performed from 100 °C to 800 °C. The CO pulse adsorption experiment was pre-treated at 300 °C for 2 h, and then pulsed with helium to 50 °C. The experiment was carried out in the CO pulse system.

## 2.3. Catalytic Oxidation Performance Evaluation

Next, 200 mg of the grinded catalyst sample with particle sizes of 40–60 mesh was weighed and put on the quartz cotton catalytic bed, which was inside the quartz tube reactor with the inner diameter of 6 mm, and the pipeline pressure was maintained at 0.2 Mpa. The weight hourly space velocity (WHSV) was set to 45,000  $\text{mL}\cdot\text{g}^{-1}\cdot\text{h}^{-1}$ , and the total intake gas flow rate was set to 150 mL/min. The concentration of DCM was 1000 ppm, the concentration of  $\text{O}_2$  was 20%, and the balance gas was  $\text{N}_2$ . Gasmeter (model Dx-4000 (GASMET, Vantaa, Finland)) was used to measure the concentration of DCM and other carbon-containing products in the outlet gas. On the basis of the following reaction Equation:  $\text{CH}_2\text{Cl}_2 + \text{O}_2 \rightarrow \text{CO}_2 + \text{CO} + \text{H}_2\text{O} + \text{HCl} + \text{Cl}_2 + \text{CH}_x\text{Cl}_y\text{O}_z$ , the DCM conversion and the  $\text{CO}_2$  selectivity ( $S_{\text{CO}_2}$ ) were calculated according to the following Equation:

$$\text{DCM} = \frac{c_{in} - c_{out}}{c_{out}} \times 100\% \quad (1)$$

$$S_{\text{CO}_2} = \frac{c_{\text{CO}_2}}{c_{in} - c_{out}} \times 100\% \quad (2)$$

where  $c_{in}$  and  $c_{out}$ , respectively, represent the intake concentration and outlet concentration of DCM.

In addition, the WHSV when measuring the turnover frequency (*TOF*) value of DCM oxidation was set to 112,500 mL·g<sup>-1</sup> h<sup>-1</sup> (80 mg catalyst sample was taken, other conditions were the same as the activity test). The calculation formula of *TOF* value is as follows:

$$TOF = \frac{X_{DCM} \times F_{DCM} \times M_{Ru}}{m_{cat} \times X_{Ru} \times D_{Ru}} \quad (3)$$

where  $X_{DCM}$  and  $X_{Ru}$ , respectively, represent the concentration of DCM and Ru, respectively,  $F_{DCM}$  represents the flow rate of DCM (mol·s<sup>-1</sup>),  $M_{Ru}$  represents the molar mass of Ru,  $D_{Ru}$  is the dispersion of Ru and  $m_{cat}$  is the mass of catalyst.

### 3. Results and Discussion

#### 3.1. DCM Catalytic Oxidation Performance Test Results

Figure 1 illustrates the DCM catalytic oxidation performance test results for each sample. Based on the carbon balance, the higher the proportion of CO<sub>2</sub> in the product, the smaller the amount of other toxic organic by-products produced. From the obtained results shown in Figure 1a, we could find that the loading of Ru can significantly improve the catalytic activity of the catalysts for DCM. It could also be found that the T<sub>90</sub> of the c-1-RuST sample was about 90 °C lower than that of the o-1-RuST sample, which was 290 °C and 380 °C, respectively. This indicated that using Ru colloid instead of the original RuO<sub>2</sub> as precursor to load active components could improve the catalytic activity of the catalyst to a large extent. By further comparing the catalytic activity of the c-1-RuST and the o-5-RuST sample (as shown in Figure S1), it could be seen that the catalytic activity of the c-1-RuST was also significantly higher than that of the o-5-RuST (T<sub>90</sub> was about 290 °C and 340 °C, respectively). Therefore, the optimization of Ru precursor could effectively reduce the loading of active components, and thus reduce the production cost of the catalyst. At the same time, it also can be found that when Ru colloid loading amount was gradually increased, the catalytic activity of the samples did not change much at first (even slightly decreased), and then showed an upward trend. Among them, the c-1-RuST sample had the best catalytic performance for DCM. As for the results showed in Figure 1b, we could find that the loading of Ru could significantly improve the CO<sub>2</sub> selectivity of the catalysts in the catalytic oxidation of DCM and there was a certain improvement of the CO<sub>2</sub> selectivity after using Ru colloid as precursor instead of RuO<sub>2</sub>. We also could find that, when increasing the loading of RuO<sub>x</sub>, the CO<sub>2</sub> selectivity of the catalysts also got a gradual improvement. The CO<sub>2</sub> selectivity of c-1-RuST sample remained higher than 80% after the temperature was higher than 300 °C, and stabilized at around 95% after the temperature reached 350 °C.

The stability test result of the c-1-RuST sample is shown in Figure 2. According to the experimental results, the c-1-RuST sample could maintain high catalytic activity (the conversion rate was always higher than 90%) and high product CO<sub>2</sub> selectivity (always above 80%) for DCM at 300 °C for more than 24 h. Therefore, it can be seen that the c-1-RuST catalyst could degrade DCM molecules stably and efficiently for a long time. At the same time, we can find that the conversion % during the stability test had increased to a certain extent. The reason might be that the surface characteristics of the catalysts had changed during the reaction, which in turn led to changes in the catalytic activity and CO<sub>2</sub> selectivity of the catalysts for the oxidation of DCM. From the point of view of the results, this change was favourable.

In order to further study the specific reasons why the optimization of Ru precursor using Ru colloid could improve the performance of the catalyst, and systematically explain the effect of RuO<sub>x</sub> loading on the performance of the catalyst, relevant characterizations on the physico-chemical properties of the catalysts were conducted.

#### 3.2. The Analysis of Physico-Chemical Properties of the Catalyst

XRD characterization was conducted on each sample to further study the effect of RuO<sub>x</sub> loading on the crystal structure under different Ru precursors and different RuO<sub>x</sub> loading conditions, the results are shown in Figure 3. Based on the information of ICSD

PDF # 76-0332, we found that all samples showed a rutile structure, showing that the loading of  $\text{RuO}_x$  did not significantly affect the crystal structure of the support for the four samples tested. The characteristic peaks of ruthenium oxide crystals were not detected for two reasons. First, the  $\text{RuO}_x$  species on the surface of the catalyst were highly dispersed in amorphous or crystalline form. Second, the crystal morphology of rutile  $\text{RuO}_x$  and  $\text{Sn}_{0.2}\text{Ti}_{0.8}\text{O}_2$  was similar to each other, with the characteristic peak positions at  $27.19^\circ$ ,  $35.69^\circ$  and  $56.08^\circ$ , which were close to the peak positions of the support and were difficult to distinguish.

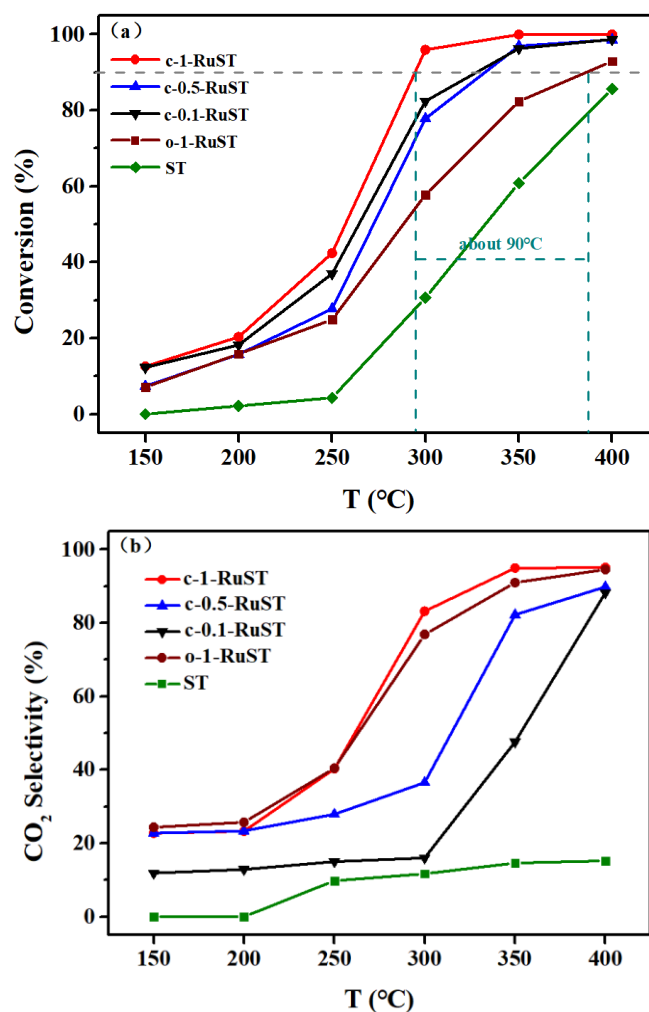


**Figure 1.** DCM catalytic oxidation performance test results for each sample: (a) DCM conversion and (b) CO<sub>2</sub> selectivity. Test conditions: (DCM) = 1000 ppm, GHSV = 45,000 mL·g<sup>-1</sup>·h<sup>-1</sup>.

From the results of TEM-Mapping showed in Figure S2, we can see that for all samples,  $\text{RuO}_x$  species were highly dispersed on the surface of the catalyst support. The research results showed that  $\text{RuO}_x$  species could grow epitaxially on the support with the same crystal structure [31], this also explained the good dispersion of  $\text{RuO}_x$  on  $\text{Sn}_{0.2}\text{Ti}_{0.8}\text{O}_2$ . The spherical aberration correction transmission electron microscope was further used to observe the size of the Ru clusters of each sample, and the experimental results are shown in Figure 4. It can be inferred from the figure that the surface of the catalyst loaded by the Ru colloid had smaller Ru clusters. Most of the Ru clusters on the surface of o-1-RuST samples were about 3–4 nm in diameter, while the Ru clusters on the surface of c-1-RuST samples were about 1.3 nm in diameter. Therefore, the optimization of Ru precursor using Ru colloid can improve the dispersity of  $\text{RuO}_x$  species, significantly improve the utilization rate of active components, and then increase the total number of active sites on the catalyst

surface. In addition, we could also find that with the increase in  $\text{RuO}_x$  loading, the size of Ru clusters on the catalyst surface gradually increased. The size of Ru clusters in the c-1-RuST sample was extremely small, and it was hard to see obvious Ru clusters, as for the c-0.5-RuST sample, there were many small Ru clusters with a diameter of about 1 nm, and the diameter of the Ru clusters on the surface of the c-1-RuST sample was about 1.3 nm. Therefore, we could see that when increasing the loading of  $\text{RuO}_x$ , the dispersibility of  $\text{RuO}_x$  species decreased by degrees, thereby reducing the utilization of active components.

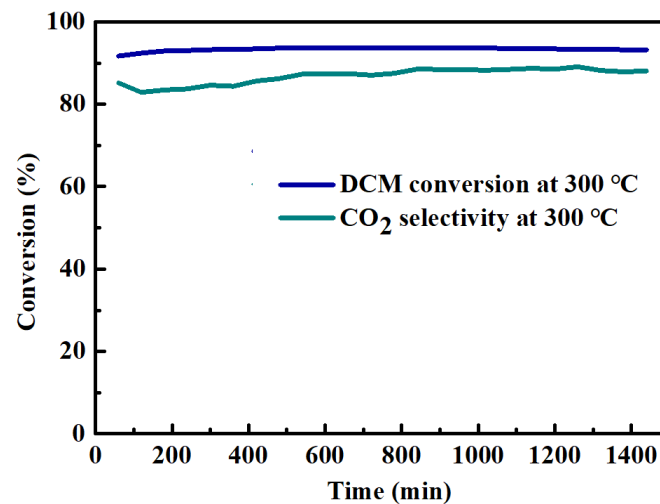


Figure 2. Stability evaluation test results of the c-1-RuST sample.

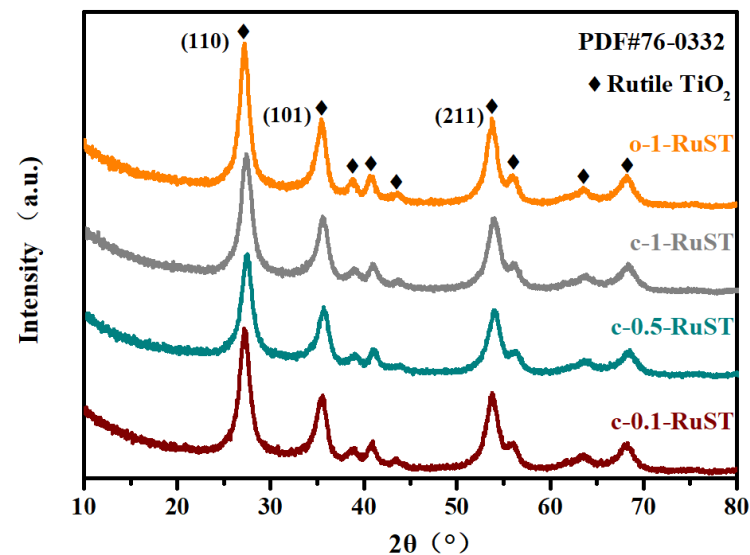
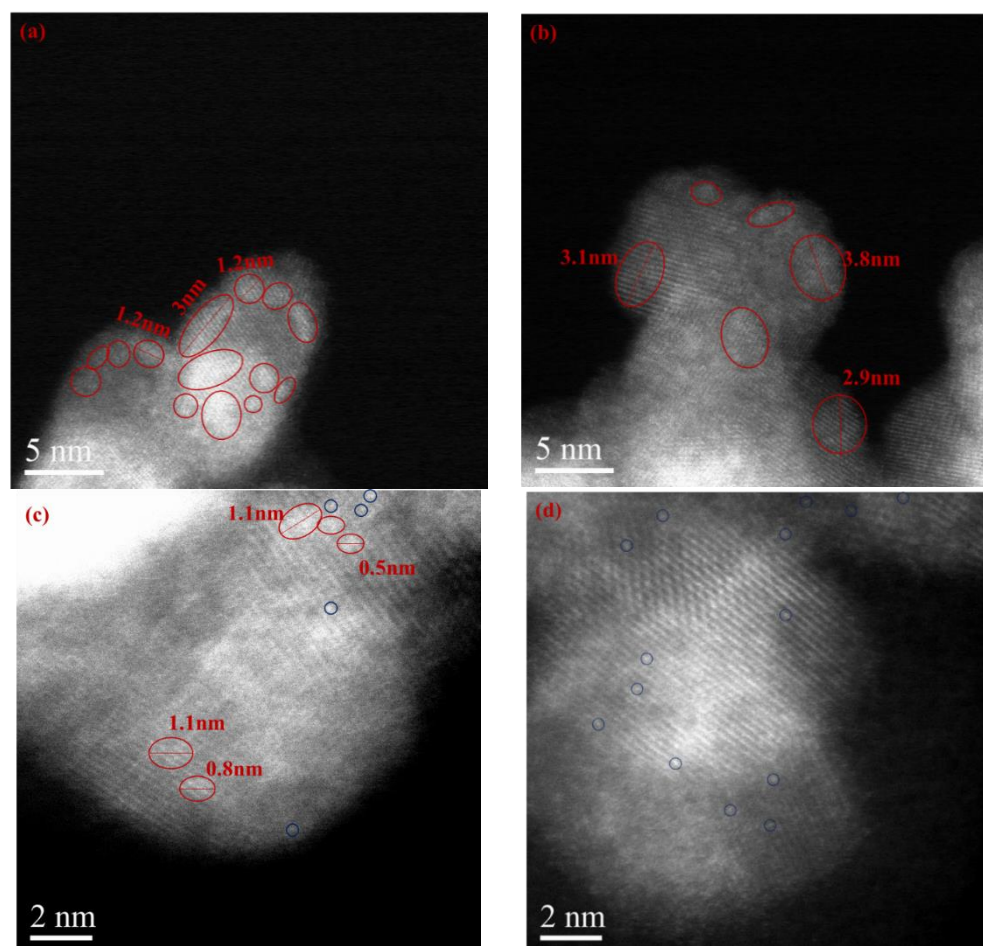


Figure 3. XRD patterns of the samples. Peak information for crystal plane acquired from the ICSD Powder Diffraction File card of Rutile  $\text{TiO}_2$  (card No. 76-0332) is also marked in the figure.

We carried out a CO pulse adsorption experiment to further verify the rule between  $\text{RuO}_x$  species dispersibility and  $\text{RuO}_x$  loading, and the results are shown in Table 1. The metal dispersion and metallic surface area of Ru in the c-0.1-RuST sample were significantly higher than those in the c-0.5-RuST sample, and the values in the c-0.5-RuST sample were also higher than those in the c-1-RuST sample. This can also explain why when increasing the loading of  $\text{RuO}_x$ , the catalytic activity of the samples did not change significantly at first and then increased. At first, as the  $\text{RuO}_x$  loading increased, the total number of  $\text{RuO}_x$  species increased but the dispersibility decreased. The effects of the two offset each other, resulting in little change in the total number of active sites of the catalyst and little

change in catalyst performance; subsequently, with the further increase in  $\text{RuO}_x$  loading, the increase in the total number of  $\text{RuO}_x$  species gradually played a dominant role, and the total number of active sites of the catalyst increased, leading to the improvement of the catalytic performance of the catalyst.



**Figure 4.** HAADF-STEM images of (a) the c-1-RuST sample, (b) the o-1-RuST sample, (c) the c-0.5-RuST sample and (d) the c-0.1-RuST sample. Representative Ru clusters and single-atom Ru in each sample and the diameters of some of the Ru clusters are also marked in the figure.

**Table 1.** CO pulse adsorption experiment results of samples with different  $\text{RuO}_x$  loadings.

Samples	Metal Dispersion (%)	Metallic Surface Area ( $\text{m}^2/\text{g}$ )
c-0.1-RuST	15.86	75.59
c-0.5-RuST	7.18	34.20
c-1-RuST	2.35	11.19

We further studied the physico-chemical properties of each sample, and some results are shown in Table 2. The molar ratio of tin to titanium ( $\text{Sn}_{\text{mol}}:\text{Ti}_{\text{mol}}$ ) of each sample was between 0.246 and 0.250, basically the same as our pre-set value (0.25), and the actual loading of Ru species also met the expectation. The deviation of the actual Ru content of some samples from the expected Ru content might be because we loaded Ru species through impregnation method, which might inevitably lead to some errors. For example, for the c-1-RuST sample, quantitative support powder and colloid solution were fully stirred in a beaker, then transferred to a flask for rotary evaporation. During this process, some Ru species might not be loaded on the surface of the catalysts. For instance, there might be

some colloidal solution containing Ru species remaining on the inner wall of the container that cannot be completely transferred. These factors inevitably caused the difference between the final loading of Ru species and the originally intended loading of Ru species, but from the XRF test results, this deviation was not very large. At the same time, the actual Ru content in the c-1-RuST sample was slightly less than that of the o-1-RuST, but its catalytic performance was much better than the latter, which also showed the superiority of the modification of the active component precursor. In addition, the BET surface area of the c-1-RuST sample was significantly larger than that of the o-1-RuST sample. At the same time, the pore size of the c-1-RuST sample was also significantly smaller than that of the o-1-RuST sample. This might be due to the fact that the particle size of Ru in Ru colloid was smaller than that in precursor of RuO<sub>2</sub>. The RuO<sub>x</sub> species in Ru colloid could distribute more evenly on the catalyst surface, and efficiently reduce the adverse effect of blocking the pore of the support on the specific surface area of the catalyst. This result is consistent with the HAADF-STEM test results. It could be seen that the optimization of Ru precursor using Ru colloid was beneficial to improve the dispersion of RuO<sub>x</sub> species, thereby increasing the total number of active sites on the catalyst surface. However, with the increase in RuO<sub>x</sub> loading, the BET surface area of the catalyst decreased slightly, indicating that the above adverse effect could not be completely eliminated.

**Table 2.** Characterization results of some physico-chemical properties of RuST series samples.

Samples	Sn <sub>mol</sub> :Ti <sub>mol</sub> <sup>a</sup>	Ru (wt%) <sup>a</sup>	BET (m <sup>2</sup> /g)	Pore Size (nm)
o-1-RuST	0.250	1.13	64.87	13.44
c-1-RuST	0.248	0.857	80.61	11.88
c-0.5-RuST	0.246	0.415	83.51	10.66
c-0.1-RuST	0.250	0.141	85.31	10.45

<sup>a</sup> Calculated from XRF measurement.

In order to explore the influence of the Ru precursor optimization on the valence state of Ru species, we performed XPS characterization. The specific data is shown in Figure 5. The binding energy of Ru<sup>4+</sup> species could be identified as 280.4 eV, and the binding energy of Ru<sup>6+</sup> species could be identified as 282.5 eV [32,33]. It can be seen from the Figure that both samples contained Ru<sup>4+</sup>, which corresponded to the crystalline RuO<sub>2</sub> or RuO<sub>2</sub> thin films on the catalyst surface. Meanwhile, Ru<sup>n+</sup> (4 < n < 6) with valence states between +4 and +6 were found in both samples. The difference was that Ru<sup>n+</sup> accounted for only 14.2% of Ru species in the o-1-RuST sample, while for c-1-RuST sample, Ru<sup>n+</sup> accounts for as much as 60.4%. Previous studies have shown that the interface charge transfer between the Ru species and the support will affect the charge density of the Ru species, and the strength of electronic interaction of strong metal-support interactions (SMSI) will directly affect the valence state of Ru on the catalyst surface [34]. Therefore, we can infer that the formation of Ru<sup>n+</sup> species was due to the close interaction between Ru and support, Ru gave electrons through the Ru–O–M (Sn, Ti) bond and thus exhibited a higher valence state than +4. The Ru clusters on the surface of the c-1-RuST sample were smaller than that in the o-1-RuST sample, and the Ru species of the c-1-RuST sample could better diffuse and distribute on the surface of catalyst, which was more conducive to the formation of bonds between Ru and other surrounding elements to form SMSI. More than half of the Ru in the c-1-RuST sample was bound to the support, which indicated that loading Ru in colloidal form greatly improved the utilization efficiency of active components, so more active sites could be formed on the catalyst surface. The specific effects of Ru<sup>n+</sup> species on the catalytic activity will be further discussed in detail in combination with the XPS results of O 1s.

The oxygen species distribution and oxygen vacancy concentration of the catalyst usually have a great impact on the catalyst oxidation performance, so we measured the valence distribution of oxygen element on the surface of each sample, and the results are shown in Figure 6. The peak value near 529.6 eV could be assigned to lattice oxygen species (O<sub>Lat</sub>), that at around 530.3 eV could be assigned to oxygen vacancy species (O<sub>V</sub>), and

that at around 531.3 eV could be classified as surface adsorbed oxygen species ( $O_{ad}$ ).  $O_{ad}$  can quickly participate in the reaction with the adsorbed DCM molecules and oxidize the reactants, thus improving the catalytic performance of the samples [35]. The oxygen vacancy concentration is very important for the adsorption and dissociation of oxygen during the reaction. Increasing the oxygen vacancy concentration can increase the oxygen transmission rate on the catalyst surface, so that the oxygen consumed by the reaction can be quickly replenished, thereby promoting the deep oxidation of DCM molecules. The oxygen vacancy concentration on the surface of each sample could be evaluated by calculating the ratio of  $O_V/O_{Lat}$  [36]. The oxygen vacancy concentration value of the o-1-RuST, the c-1-RuST, the c-0.5-RuST and the c-0.1-RuST sample was 1.44, 1.53, 1.47 and 1.50, respectively. Comparing the O1s spectra of the o-1-RuST and the c-1-RuST samples, we could find that the c-1-RuST sample had more  $O_{ad}$  and a higher oxygen vacancy concentration on the surface, which was consistent with the catalytic activity and  $CO_2$  selectivity test results of the two samples. The distribution of  $RuO_x$  species on the surface of the c-1-RuST sample was more uniform, which helped to adsorb more oxygen; at the same time, the c-1-RuST sample had a higher proportion of  $Ru^{n+}$ , the forming of Ru–O–M (Sn, Ti) bonds could significantly increase the oxygen vacancy concentration [37,38]; the above two points encouraged the catalyst toward a better redox performance, and thus had better low-temperature catalytic activity and  $CO_2$  selectivity [39]. Therefore, we can infer that the optimization of the Ru precursor was beneficial to increase the number of active oxidation sites of the catalyst, thus helping to improve the overall catalytic performance of the catalyst.

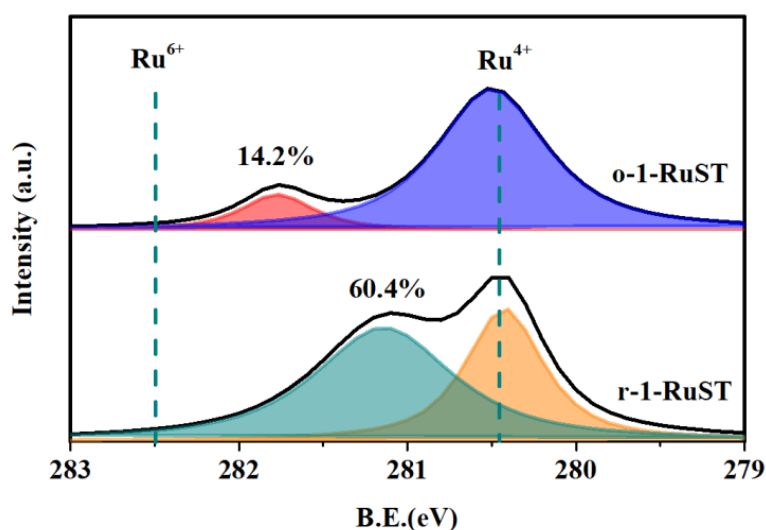


**Figure 5.** XPS data of Ru 3d for the c-1-RuST sample and o-1-RuST sample. The peak positions of  $Ru^{4+}$  and  $Ru^{6+}$  binding energy and the ratio of  $Ru^{n+}$  ( $4 < n < 6$ ) to the total number of Ru species in the two samples are also marked in the Figure.

Comparing the O1s spectra of the three samples of the c-1-RuST, the c-0.5-RuST, and the c-0.1-RuST, it could be concluded that when the Ru loading was increased, the  $O_{ad}$  content of the catalyst gradually increased, which showed that the  $RuO_x$  species on the catalyst surface was the key sites for the adsorption of environmental oxygen. Furthermore, the oxygen vacancy concentration of each sample followed the c-1-RuST > the c-0.1-RuST > the c-0.5-RuST, this might be because the c-0.1-RuST sample had the smallest size of Ru clusters and the smaller size of Ru clusters could show stronger electron interaction with the support [36]. At the same time, this result was consistent with the test results of the catalytic performance of each sample for DCM, suggesting that the c-0.1-RuST sample with better  $RuO_x$  species dispersibility had a higher utilization efficiency of active components and had a larger total number of active sites of the catalyst than the c-0.5-RuST sample.

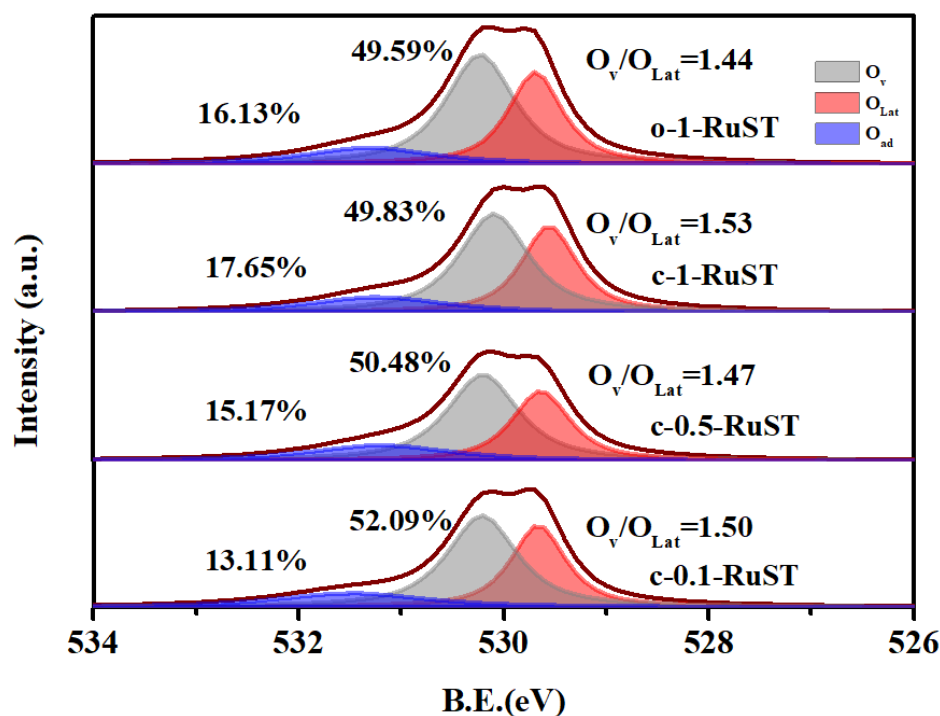


**Figure 6.** XPS data of O 1s for the samples. The proportion of  $O_{ad}$  and  $O_v$  in the total number of oxygen species in each sample and the oxygen vacancy concentration ( $O_v/O_{Lat}$ ) of each sample are also marked in the Figure.

The slight shift of the binding energy peak value of oxygen species in each sample showed that there were differences in the electronic environment of oxygen atoms in different samples. The difference in strength of the interaction between the Ru species and the support in different samples might be the reason for this phenomenon. The binding energy of oxygen species in the c-1-RuST sample was lower than that in the o-1-RuST sample, which was consistent with the results of HAADF-STEM images and XPS data of Ru 3d. In c-1-RuST sample; there was a stronger interaction between Ru species and the support, forming more Ru-O-M bonds, resulting in more electron transfer from Ru to O and a decrease in the binding energy of oxygen species. The order of binding energy of oxygen species in the c-1-RuST, the c-0.5-RuST, and the c-0.1-RuST sample was the same as the order of oxygen vacancy concentration. This could be explained by the fact that the c-0.1-RuST sample had the smallest size of Ru clusters, which had a stronger interaction with the support, but the Ru content of the c-1-RuST sample was much greater than that of the c-0.1-RuST sample.

In order to further explore the redox performance of the catalysts, we performed  $H_2$ -TPR characterization on the samples, and the results are shown in Figure 7. Observing the image, we could find that the four samples all had a reduction peak at 250 °C to 400 °C and this can be attributed to the reduction of  $Sn^{4+}$  [20]. The reduction peak from 450 °C to 750 °C can be attributed to the reduction of bulk oxygen in the support [40]. It can be found that the reduction peak of this part was basically the same for each sample. The reduction peak located near 240 °C was caused by the reduction of oxygen on the catalyst surface [40], which varied greatly among different samples. The reduction peak area of the c-1-RuST sample near 240 °C was significantly larger than that of the o-1-RuST sample, indicating that the c-1-RuST sample had more surface oxygen, which was consistent with the results of  $CO_2$  selectivity and XPS data of O 1s. This showed that the smaller and more uniformly distributed  $RuO_x$  in the c-1-RuST sample could form more oxidation active sites and absorb more environmental oxygen, thus improving the oxidation-reduction performance of the catalyst. At the same time, comparing the samples of the c-1-RuST, the c-0.5-RuST and the c-0.1-RuST, it could be seen that with the increase in  $RuO_x$  species

loading, the oxygen content on the catalyst surface gradually increased, showing that the total amount of oxygen increased with the increase in  $\text{RuO}_x$  loading, which is also coincide to the  $\text{CO}_2$  selectivity results of each sample. It was difficult to observe obvious  $\text{RuO}_x$  species reduction peaks in the image, because the content of  $\text{RuO}_x$  species in the samples was too low, and the reduction peak of Ru species was close to the reduction peak of surface oxygen.

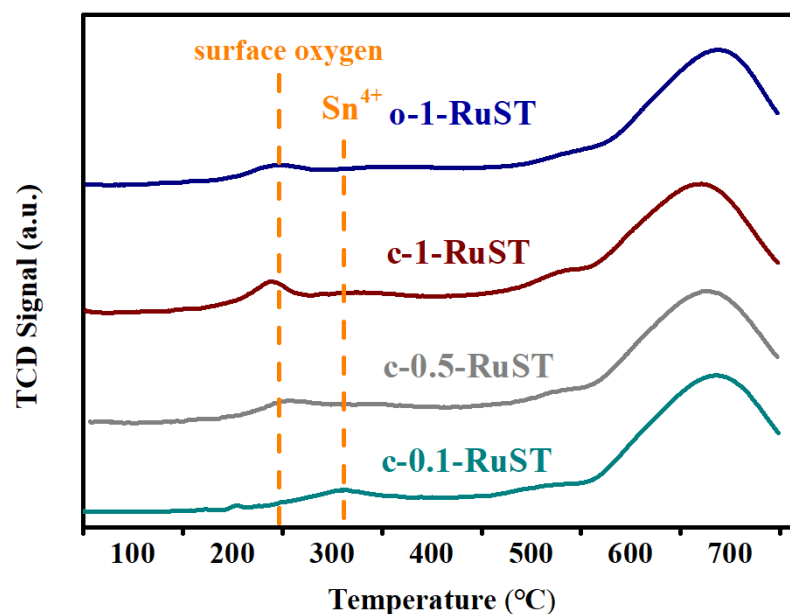


**Figure 7.**  $\text{H}_2$ -TPR profiles of the catalysts. The reduction peak positions of  $\text{Sn}^{4+}$  and oxygen species on the catalyst surface are also marked in the figure.

In order to verify the effect of optimization of Ru precursor on the utilization efficiency of active sites and the overall catalytic performance of the catalyst, we calculated the TOF values of the c-1-RuST sample and the o-1-RuST sample at 230–280 °C, and the results are shown in the Figure 8. The experimental WHSV was maintained at  $112,500 \text{ mL}\cdot\text{g}^{-1}\cdot\text{h}^{-1}$ , and the DCM conversion rate was controlled to be less than 20%, so that the reaction rate was not affected by diffusion, and only depended on the number of active sites. It can be seen from the experimental calculation results that the TOF value of the c-1-RuST sample for DCM was always significantly higher than that of the o-1-RuST sample, even up to about twice the value (for example, at 270 °C, the TOF value of the c-1-RuST sample was 0.20, and which of the o-1-RuST sample was 0.12). In conclusion, loading Ru species in the form of Ru colloid could improve the catalytic performance of a single active site, and then improve the overall catalytic activity of the samples. Based on the results of the previous characterization analysis, the reason may be that the optimization of Ru precursor could help to improve the dispersion of  $\text{RuO}_x$  species on the catalyst surface, thus promoting a larger proportion of Ru species to form Ru–O–M bonds with the support, generating more  $\text{Ru}^{n+}$  ( $4 < N < 6$ ). This change significantly increased the adsorbed oxygen content and oxygen vacancy concentration on the catalyst surface, thus leading to the improvement of the catalyst oxidation performance. Therefore, under the condition of similar  $\text{RuO}_x$  loading, the c-1-RuST sample with higher  $\text{RuO}_x$  species utilization rate could catalyse and oxidize more DCM molecules in the same experimental conditions.

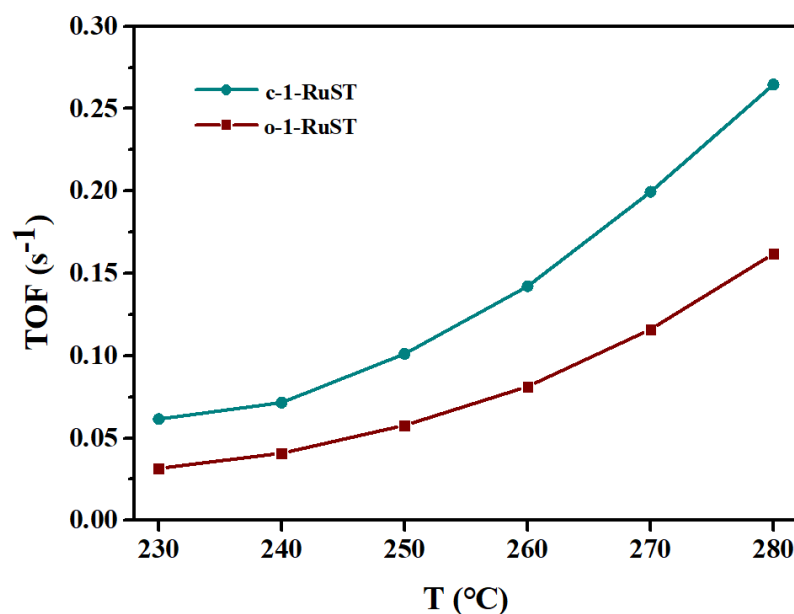


**Figure 8.** TOF for DCM oxidation on the c-1-RuST and the o-1-RuST sample. Test conditions: [DCM] = 1000 ppm, WHSV = 112,500 mL·g<sup>-1</sup>·h<sup>-1</sup>.

#### 4. Conclusions

In this article, the Ru precursor was optimized using Ru colloid and a unique catalyst preparation method was developed. The Ru species was loaded on the Sn<sub>0.2</sub>Ti<sub>0.8</sub>O<sub>2</sub> support in colloidal form, which improved the utilization efficiency of active components, and effectively improved the catalytic activity ( $T_{90}$  was reduced by about 90 °C from 380 °C to 290 °C) and the CO<sub>2</sub> selectivity. Through the activity test and various characterization analyses, it could be concluded that the optimization of Ru precursor could significantly increase the dispersion of RuO<sub>x</sub> species (the size of Ru clusters was reduced from 3–4 nm to about 1.3 nm), improve the utilization of active components (nearly doubled the TOF value at each temperature measured), and increase the interaction between the active components and the support. This improvement effectively increased the total number of active sites of the catalyst, thus improving the catalyst oxidation capability.

In addition, for the sake of better determining the optimal Ru loading, the relationship between the Ru loading and the catalytic activity of the catalyst was further studied. The experimental results reflected that with the increase in Ru loading, the total amount of RuO<sub>x</sub> species on the catalyst surface increased, while the dispersibility of that gradually decreased. This resulted in little change in the total number of active sites of the catalyst, and little change in the catalytic activity of the samples ( $T_{90}$  of the c-0.1-RuST and the c-0.5-RuST for DCM was about 330 °C and 335 °C respectively) when the content of Ru was low (less than 0.5 wt%). When the content of Ru was high (above than 0.5 wt%), the positive effect caused by the increase in the total active component amount gradually played a leading role, and the catalytic performance of the catalyst was significantly improved.

In conclusion, the study is conducive to the efficient treatment of CVOCs and can provide theoretical guidance for further reducing the content of active components (the Ru loading could be reduced from about 5% to less than 1%) and production cost, thus having broad industrial application prospects.

**Supplementary Materials:** The following are available online at <https://www.mdpi.com/article/10.3390/catal11111306/s1>, Figure S1 Results of catalytic performance evaluation for DCM oxidation over the c-1-RuST and the o-1-RuST sample. Test conditions: (DCM) = 1000 ppm; WHSV = 45,000 mL·g<sup>-1</sup>·h<sup>-1</sup>, Figure S2 EDS-Mapping characterization results of (a) the c-1-RuST sample, (b) the o-1-RuST sample, (c) the c-0.5-RuST sample and (d) the c-0.1-RuST sample, Table S1 Chemical reagents used in catalyst preparation.

**Author Contributions:** Conceptualization, Y.Y. and X.Y.; methodology, Z.Z.; software, M.K.; validation, S.L.; formal analysis, Z.Z.; investigation, Z.Z.; resources, X.Y.; data curation, Z.H.; writing—original draft preparation, Z.Z.; writing—review and editing, Y.Y.; visualization, Z.Y.; supervision, Y.J.; project administration, X.G.; funding acquisition, X.G. All authors have read and agreed to the published version of the manuscript.

**Funding:** This research was funded by the [National Natural Science Foundation of China] grant number [No.51836006] and [No.52006192] and [Qingdao Science and Technology Demonstration and Guidance Project] grant number [21-1-4-sf-8-nsh].

**Conflicts of Interest:** The authors declare no conflict of interest.

## References

1. Geng, C.; Yang, W.; Sun, X.; Wang, X.; Bai, Z.; Zhang, X. Emission factors, ozone and secondary organic aerosol formation potential of volatile organic compounds emitted from industrial biomass boilers. *J. Environ. Sci.* **2019**, *83*, 64–72. [[CrossRef](#)] [[PubMed](#)]
2. Amnuaylojaroen, T.; Macatangay, R.C.; Khodmanee, S. Modeling the effect of VOCs from biomass burning emissions on ozone pollution in upper Southeast Asia. *Heliyon* **2019**, *5*, e02661. [[CrossRef](#)]
3. Liu, Y.; Song, M.; Liu, X.; Zhang, Y.; Hui, L.; Kong, L.; Zhang, Y.; Zhang, C.; Qu, Y.; An, J.; et al. Characterization and sources of volatile organic compounds (VOCs) and their related changes during ozone pollution days in 2016 in Beijing, China. *Environ. Pollut.* **2019**, *257*, 113599. [[CrossRef](#)] [[PubMed](#)]
4. Doucette, W.J.; Wetzel, T.A.; Dettenmaier, E.; Gorder, K. Emission rates of chlorinated volatile organics from new and used consumer products found during vapor intrusion investigations: Impact on indoor air concentrations. *Environ. Forensics* **2018**, *19*, 185–190. [[CrossRef](#)]
5. Hossaini, R.; Chipperfield, M.; Montzka, S.A.; Leeson, A.; Dhomse, S.S.; Pyle, J.A. The increasing threat to stratospheric ozone from dichloromethane. *Nat. Commun.* **2017**, *8*, 15962. [[CrossRef](#)]
6. Blanch-Raga, N.; Palomares, A.E.; Triguero, J.M.; Puche, M.; Fetter, G.; Bosch, P. The oxidation of trichloroethylene over different mixed oxides derived from hydrotalcites. *Appl. Catal. B Environ.* **2014**, *160–161*, 129–134. [[CrossRef](#)]
7. Dobrzyńska, E.; Pośniak, M.; Szewczyńska, M.; Buszewski, B. Chlorinated Volatile Organic Compounds—Old, However, Actual Analytical and Toxicological Problem. *Crit. Rev. Anal. Chem.* **2010**, *40*, 41–57. [[CrossRef](#)]
8. Krol, M.C.; Lelieveld, J.; Oram, D.E.; Sturrock, G.A.; Penkett, S.A.; Brenninkmeijer, C.A.M.; Gros, V.; Williams, J.; Scheeren, H.A. Continuing emissions of methyl chloroform from Europe. *Nature* **2003**, *421*, 131–135. [[CrossRef](#)]
9. Li, C.; Zhao, Y.; Song, H.; Li, H. A review on recent advances in catalytic combustion of chlorinated volatile organic compounds. *J. Chem. Technol. Biotechnol.* **2019**, *95*, 2069–2082. [[CrossRef](#)]
10. Zheng, Z.; Yang, Y.; Li, H.; Xin, Q.; Zhang, S.; Liu, Y.; Liu, S.; Zheng, C.; Song, H.; Gao, X. Effect of multi-pollutant on the catalytic oxidation of dichloromethane over RuO<sub>2</sub>-WO<sub>3</sub>/Sn<sub>0.2</sub>Ti<sub>0.8</sub>O<sub>2</sub> catalyst. *Fuel* **2020**, *278*, 118207. [[CrossRef](#)]
11. Yang, Y.; Liu, S.; Zhao, H.; Li, H.; Qu, R.; Zhang, S.; Zhu, X.; Zheng, C.; Gao, X. Promotional effect of doping Cu into cerium-titanium binary oxides catalyst for deep oxidation of gaseous dichloromethane. *Chemosphere* **2018**, *214*, 553–562. [[CrossRef](#)] [[PubMed](#)]
12. Tian, M.; Guo, X.; Dong, R.; Guo, Z.; Shi, J.; Yu, Y.; Cheng, M.; Albilali, R.; He, C. Insight into the boosted catalytic performance and chlorine resistance of nanosphere-like meso-macroporous CrO<sub>x</sub>/MnCo<sub>3</sub>O<sub>x</sub> for 1,2-dichloroethane destruction. *Appl. Catal. B Environ.* **2019**, *259*, 118018. [[CrossRef](#)]
13. Aouad, S.; Abi-Aad, E.; Aboukais, A. Simultaneous oxidation of carbon black and volatile organic compounds over Ru/CeO<sub>2</sub> catalysts. *Appl. Catal. B Environ.* **2009**, *88*, 249–256. [[CrossRef](#)]
14. Okal, J.; Zawadzki, M. Influence of Catalyst Pretreatments on Propane Oxidation Over Ru/gamma-Al<sub>2</sub>O<sub>3</sub>. *Catal. Lett.* **2009**, *132*, 225–234. [[CrossRef](#)]
15. Joo, S.H.; Park, J.Y.; Renzas, J.; Butcher, D.R.; Huang, W.; Somorjai, G.A. Size Effect of Ruthenium Nanoparticles in Catalytic Carbon Monoxide Oxidation. *Nano Lett.* **2010**, *10*, 2709–2713. [[CrossRef](#)] [[PubMed](#)]
16. Chen, H.-T. First-Principles Study of CO Adsorption and Oxidation on Ru-Doped CeO<sub>2</sub>(111) Surface. *J. Phys. Chem. C* **2012**, *116*, 6239–6246. [[CrossRef](#)]
17. Hevia, M.A.; Amrute, A.P.; Schmidt, T.; Pérez-Ramírez, J. Transient mechanistic study of the gas-phase HCl oxidation to Cl<sub>2</sub> on bulk and supported RuO<sub>2</sub> catalysts. *J. Catal.* **2010**, *276*, 141–151. [[CrossRef](#)]
18. Sun, W.; Gong, B.; Pan, J.; Wang, Y.; Xia, H.; Zhang, H.; Dai, Q.; Wang, L.; Wang, X. Catalytic combustion of CVOCs over Cr<sub>x</sub>Ti<sub>1-x</sub> oxide catalysts. *J. Catal.* **2020**, *391*, 132–144. [[CrossRef](#)]
19. Lv, X.; Cai, S.; Chen, J.; Yan, D.; Jiang, M.; Jia, H. Tuning the degradation activity and pathways of chlorinated organic pollutants over CeO<sub>2</sub> catalyst with acid sites: Synergistic effect of Lewis and Brønsted acid sites. *Catal. Sci. Technol.* **2021**. [[CrossRef](#)]
20. Yang, Y.; Li, H.; Zhao, H.; Qu, R.; Zhang, S.; Hu, W.; Yu, X.; Zhu, X.; Liu, S.; Zheng, C.; et al. Structure and crystal phase transition effect of Sn doping on anatase TiO<sub>2</sub> for dichloromethane decomposition. *J. Hazard. Mater.* **2019**, *371*, 156–164. [[CrossRef](#)]
21. Chen, X.; Zhao, Z.; Zhou, Y.; Zhu, Q.; Pan, Z.; Lu, H. A facile route for spraying preparation of Pt/TiO<sub>2</sub> monolithic catalysts toward VOCs combustion. *Appl. Catal. A Gen.* **2018**, *566*, 190–199. [[CrossRef](#)]

22. Todorova, S.; Blin, J.; Naydenov, A.; Lebeau, B.; Kolev, H.; Gaudin, P.; Dotzeva, A.; Velinova, R.; Filkova, D.; Ivanova, I.; et al.  $\text{Co}_3\text{O}_4\text{-MnO}_x$  oxides supported on SBA-15 for CO and VOCs oxidation. *Catal. Today* **2019**, *357*, 602–612. [[CrossRef](#)]
23. Topka, P.; Dvořáková, M.; Kšířová, P.; Perekrestov, R.; Čada, M.; Balabánová, J.; Koštejn, M.; Jiráťová, K.; Kovanda, F. Structured cobalt oxide catalysts for VOC abatement: The effect of preparation method. *Environ. Sci. Pollut. Res.* **2019**, *27*, 7608–7617. [[CrossRef](#)]
24. Wang, F.; Li, Z.; Wang, H.; Chen, M.; Zhang, C.; Ning, P.; He, H. Nano-sized Ag rather than single-atom Ag determines CO oxidation activity and stability. *Nano Res.* **2021**, 1–5. [[CrossRef](#)]
25. Veisi, H.; Azizi, S.; Mohammadi, P. Green synthesis of the silver nanoparticles mediated by *Thymra spicata* extract and its application as a heterogeneous and recyclable nanocatalyst for catalytic reduction of a variety of dyes in water. *J. Clean. Prod.* **2018**, *170*, 1536–1543. [[CrossRef](#)]
26. Xu, L.; Chen, D.; Qu, J.; Wang, L.; Tang, J.; Liu, H.; Yang, J. Replacement reaction-based synthesis of supported palladium catalysts with atomic dispersion for catalytic removal of benzene. *J. Mater. Chem. A* **2018**, *6*, 17032–17039. [[CrossRef](#)]
27. Agarwal, N.; Freakley, S.J.; McVicker, R.U.; Althahban, S.M.; Dimitratos, N.; He, Q.; Morgan, D.J.; Jenkins, R.L.; Willock, D.J.; Taylor, S.H.; et al. Aqueous Au-Pd colloids catalyze selective  $\text{CH}_4$  oxidation to  $\text{CH}_3\text{OH}$  with  $\text{O}_2$  under mild conditions. *Science* **2017**, *358*, 223–227. [[CrossRef](#)] [[PubMed](#)]
28. Zhao, Y.; Jia, L.; Medrano, J.A.; Ross, J.R.H.; Lefferts, L. Supported Pd Catalysts Prepared via Colloidal Method: The Effect of Acids. *ACS Catal.* **2013**, *3*, 2341–2352. [[CrossRef](#)]
29. Zhao, Y.; Chen, D.; Liu, J.; He, D.; Cao, X.; Han, C.; Lu, J.; Luo, Y. Tuning the metal-support interaction on chromium-based catalysts for catalytically eliminate methyl mercaptan: Anchored active chromium species through surface hydroxyl groups. *Chem. Eng. J.* **2020**, *389*, 124384. [[CrossRef](#)]
30. Li, H.; Wang, G.; Zhang, F.; Zou, L.; Zou, Z.; Yang, H. An Atomically Dispersed Pt Catalyst Anchored on an Fe/N/C Support for Enhanced Hydrogen Evolution Reaction. *J. Phys. Chem. C* **2020**, *124*, 11760–11766. [[CrossRef](#)]
31. Seitsonen, A.P.; Over, H. Oxidation of HCl over  $\text{TiO}_2$ -Supported  $\text{RuO}_2$ : A Density Functional Theory Study. *J. Phys. Chem. C* **2010**, *114*, 22624–22629. [[CrossRef](#)]
32. Nong, S.; Dong, W.; Yin, J.; Dong, B.; Lu, Y.; Yuan, X.; Wang, X.; Bu, K.; Chen, M.; Jiang, S.; et al. Well-Dispersed Ruthenium in Mesoporous Crystal  $\text{TiO}_2$  as an Advanced Electrocatalyst for Hydrogen Evolution Reaction. *J. Am. Chem. Soc.* **2018**, *140*, 5719–5727. [[CrossRef](#)] [[PubMed](#)]
33. National Institute of Standards and Technology. *NIST X-ray Photoelectron Spectroscopy Database, Version 4.1*; National Institute of Standards and Technology: Gaithersburg, MD, USA, 2012. Available online: <http://srdata.nist.gov/xps/> (accessed on 20 April 2020).
34. Guo, Y.; Mei, S.; Yuan, K.; Wang, D.J.; Liu, H.C.; Yan, C.H.; Zhang, Y.W. Low-Temperature  $\text{CO}_2$  Methanation over  $\text{CeO}_2$ -Supported Ru Single Atoms, Nanoclusters, and Nanoparticles Competitively Tuned by Strong Metal-Support Interactions and H-Spillover Effect. *ACS Catal.* **2018**, *8*, 6203–6215. [[CrossRef](#)]
35. Yang, Y.; Li, H.; Zhang, S.; Yu, X.; Liu, S.; Qu, R.; Zheng, C.; Gao, X. Different reactive behaviours of dichloromethane over anatase  $\text{TiO}_2$  supported  $\text{RuO}_2$  and  $\text{V}_2\text{O}_5$ . *Catal. Today* **2019**, *355*, 349–357. [[CrossRef](#)]
36. Li, J.; Liu, Z.; Cullen, D.A.; Hu, W.; Huang, J.; Yao, L.; Peng, Z.; Liao, P.; Wang, R. Distribution and Valence State of Ru Species on  $\text{CeO}_2$  Supports: Support Shape Effect and Its Influence on CO Oxidation. *ACS Catal.* **2019**, *9*, 11088–11103. [[CrossRef](#)]
37. Liotta, L.; Ousmane, M.; Di Carlo, G.; Pantaleo, G.; Deganello, G.; Marcì, G.; Retailleau, L.; Giroir-Fendler, A. Total oxidation of propene at low temperature over  $\text{Co}_3\text{O}_4\text{-CeO}_2$  mixed oxides: Role of surface oxygen vacancies and bulk oxygen mobility in the catalytic activity. *Appl. Catal. A Gen.* **2008**, *347*, 81–88. [[CrossRef](#)]
38. Pu, Z.-Y.; Liu, X.-S.; Jia, A.-P.; Xie, Y.-L.; Lu, J.-Q.; Luo, M.-F. Enhanced Activity for CO Oxidation over Pr- and Cu-Doped  $\text{CeO}_2$  Catalysts: Effect of Oxygen Vacancies. *J. Phys. Chem. C* **2008**, *112*, 15045–15051. [[CrossRef](#)]
39. Dai, Q.; Wu, J.; Deng, W.; Hu, J.; Wu, Q.; Guo, L.; Sun, W.; Zhan, W.; Wang, X. Comparative studies of P/ $\text{CeO}_2$  and Ru/ $\text{CeO}_2$  catalysts for catalytic combustion of dichloromethane: From effects of  $\text{H}_2\text{O}$  to distribution of chlorinated by-products. *Appl. Catal. B Environ.* **2019**, *249*, 9–18. [[CrossRef](#)]
40. Li, J.; Liu, Z.; Wang, R. Support structure and reduction treatment effects on CO oxidation of  $\text{SiO}_2$  nanospheres and  $\text{CeO}_2$  nanorods supported ruthenium catalysts. *J. Colloid Interface Sci.* **2018**, *531*, 204–215. [[CrossRef](#)]